MULTI-VIEW THROUGH-THE-WALL RADAR IMAGING USING COMPRESSED SENSING

Jie Yang[1], *Abdesselam Bouzerdoum*[1], *and Moeness G. Amin*[2]

[1]School of Electrical, Computer & Telecommunications Engineering,
University of Wollongong, Wollongong, NSW 2522, Australia

[2]Centre for Advanced Communications, Villanova University
Villanova, PA 19085, USA

Email: jy962@uow.edu.au, a.bouzerdoum@uow.edu.au, moeness.amin@villanova.edu

ABSTRACT

This paper considers the problem of Through-the-Wall Radar Imaging (TWRI) from multiple views using Compressed Sensing (CS). The scene reconstruction problem is reformulated in terms of finding a sparse representation of the target locations, consistent with the observations. In contrast to the common approach of first applying image formation to each view and then fusing the single-view images, observations from the different views are combined together into a composite measurement vector and a new dictionary is constructed accordingly. A sparse image representation of the scene is then obtained from the composite measurement vector and the new dictionary using ℓ_1-norm minimization. Experimental results demonstrate that the proposed approach using various standoff distances and perspectives achieves a better performance in terms of detecting targets compared to the alternative approach of image formation followed by fusion.

1. INTRODUCTION

Through-the-Wall Radar Imaging (TWRI) is emerging as a viable technology for producing high quality imagery of enclosed structures. Much attention has been paid to TWRI in recent years due to its ability to "see" through walls and opaque materials. TWRI makes use of electromagnetic waves below the S-band to penetrate through building wall materials to illuminate an indoor scene. A plethora of signal processing techniques has been developed for the image reconstruction, target detection, classification and tracking using TWRI; see [1, 2] and references therein for more details on TWRI and its potential applications. There is, however, increasing demands on TWRI systems to produce high resolution images in shorter acquisition times. High resolution in both down-range and cross-range requires Ultrawide frequency band and long antenna arrays to be synthesized [3], which increases the time of data acquisition and processing, not to mention cost.

Compressed sensing (CS) has received considerable attention recently for its ability to perform data acquisition and compression simultaneously [4–6]. It can reconstruct a sparse approximation of a compressible signal (or a scene) from far fewer measurements than required by the sampling theorem. This has the advantage of reducing the data acquisition time and, at the same time, improving the image quality. More recently, it has been applied to image formation in TWRI [7–9] and stepped-frequency ground penetrating radar [10]. It has been shown that if the scene contains a small number of point-like targets, it is sufficient to reconstruct the image from few random measurements. Moreover, images obtained using CS exhibit less clutter, higher resolution, and are more robust to noise compared to those obtained using traditional beamforming and backprojection methods.

One problem associated with the received data is that signals are corrupted by noise and other effects such as layover and shadows. For example, large metallic objects may obscure smaller targets placed behind. Combining multiple views of the same scene reveals hidden targets and offers the opportunity to improve the accuracy and completeness of the reconstructed image. When a sequence of raw data representing the same region of interest is collected from different views, the question of how to make proper use of the observations plays a fundamental role in the fusion process. Usually, the fusion strategy is problem-dependent and requires some *a priori* knowledge. In TWRI, fusion techniques have been so far applied to images obtained using beamforming. In [3], fusion of TWRI data is implemented by a pixel-wise multiplication scheme. Although this approach is simple and low-cost, it only performs better than a single view when the targets return strong reflections in all the received radar signals. Also, due to the adopted thresholding scheme, a too low or too high threshold may cause false detections or false rejections. In [11], a hypothesis testing approach, based on the Neyman-Pearson test, was developed for target detection from multiple views; however this approach relies on knowledge of the models or reliable estimates of the statistics of clutter, noise, and targets. More importantly, in the previous two methods, fusion is effected after each image corresponding to a single view has been aligned and image registration has been properly performed.

In this paper, a new approach for multi-view TWRI based on compressed sensing is proposed. So far all CS techniques developed for radar imaging have been applied to the single

 ISSN 2076-1465

view image reconstruction. Here, CS is applied to the combined measurement data from several views. The views can represent different locations of the imaging system along the same wall or from different sides of the building. The remainder of the paper is organized as follows. Section 2 gives a brief introduction to wideband beamforming for single-view TWRI. Section 3 presents the proposed approach for multiple-view TWRI, which is followed by a comparison between the proposed CS-based algorithm and the traditional approach for TWRI fusion. Finally, Section 5 presents some concluding remarks.

2. WIDEBAND BEAMFORMING FOR TWRI

High resolution SAR (synthetic aperture radar) imagery has extensively been considered as a source for detection and reconstruction of human scale features. In [12], synthetic aperture beamforming was applied to through-the-wall radar imaging. While high cross-range resolution is obtained by synthesizing a larger aperture, the down-range resolution is improved by increasing the signal bandwidth. In the stepped frequency approach, a large bandwidth is achieved by transmitting N narrowband signals of frequency,

$$f_n = f_0 + n\Delta f, \text{ for } n = 0,1,\ldots,N-1, \tag{1}$$

where f_0 is the first frequency and Δf is the frequency step. Consider the region of interest (ROI) to be imaged as a rectangle of size $N_x \times N_y$, where N_x and N_y denote the spatial resolutions along the *x*- and *y*-axis, respectively. Suppose an *M*-array of transmit/receive antennas, each operating with N frequencies, is placed parallel to the wall along the *x* direction. The reflections from any targets inside the ROI would be collected by each antenna. Given *P* targets in the scene, the reflected signal for frequency f_n received by the *m*th antenna can be expressed as follows:

$$z[m,n] = \sum_{p=1}^{P} \sigma_p \exp(-j2\pi f_n \tau_{pm}), \tag{2}$$

where σ_p is the reflection coefficient of the *p*th target, and τ_{pm} denotes the round-trip propagation delay between the *p*th target and the *m*th transmit/receive antenna. Here, we assume a monostatic operation. Let l_{m1} and l_{m2} be the distances traveled through the walls, and let r_{m1} and r_{m2} be the distances traveled in the air, in both transmit and receive directions, respectively. (We should note that for monostatic operations, transmit and receive distances are equal.) The round-trip time delay τ_{pm} is given by

$$\tau_{pm} = \frac{l_{m1} + l_{m2}}{v} + \frac{r_{m1} + r_{m2}}{c}$$

where c is the velocity of light in the air, $v = c/\sqrt{\varepsilon}$ is the velocity inside the wall, and ε is the dielectric constant. The image of a pixel at location (i, j) is formed by combining all the signals recorded at the *M* receivers. Using delay-and-sum beamforming, the complex amplitude of the pixel $s[i, j]$ is

$$s[i,j] = \frac{1}{MN} \sum_{m=1}^{M} \sum_{n=1}^{N} z[m,n] \exp(j2\pi f_n \tau_{m,ij}), \tag{3}$$

where $\tau_{m,ij}$ is the two-way propagation time between the the *ij*th pixel and the *m*th antenna. The total number of data points used in (3) is $M \times N$, which is equal to the number of antennas times the number of frequencies. Equation (3) also represents the frequency domain backprojection method.

3. COMPRESSED SENSING FOR TWRI

3. 1 CS and its application in single-view TWRI

With the rapidly increasing demand on large-scale signal processing, it is not surprising to see compressed sensing emerging as one of the most important research areas in the past decade. CS can reconstruct a sparse signal from small number of nonadaptive linear projections, or measurements. Consider the previous through-the-wall radar image formation problem again. Since the number of enclosed targets is fewer than the number of pixels, the image formation problem in TWRI can be formulated as a CS problem.

Let s_{ij} be an indicator function

$$s_{ij} = \begin{cases} \sigma_p, & \text{if a target exists at pixel } ij \\ 0, & \text{if there is no target} \end{cases} \tag{4}$$

The elements s_{ij} are arranged into a column vector $\boldsymbol{s}$ by a lexicographical ordering. The measurement $z[m,n]$ given in Eq. (2) can be expressed as

$$z[m,n] = \psi_{m,n} \boldsymbol{s},$$

where $\psi_{m,n} = \exp(-j2\pi f_n \tau_{m,ij})$ is a row vector. Therefore, the data vector $\boldsymbol{z}$, obtained by a lexicographical ordering of the measurements $z[m,n]$, can be expressed as

$$\boldsymbol{z} = \psi \boldsymbol{s}.$$

The vector $\boldsymbol{z}$ has length MN. Given a measurement matrix Φ of size $K \times MN$ (with $K < MN$), we can write

$$\boldsymbol{y} = \Phi \psi \boldsymbol{s} = A\boldsymbol{s} \tag{5}$$

Compressed sensing seeks to

$$\min \|\boldsymbol{s}\|_1 \quad \text{subject to} \quad \boldsymbol{y} = A\boldsymbol{s} \tag{6}$$

where $\|\cdot\|_1$ denotes the ℓ_1 norm.

The problem now consists of designing a measurement matrix Φ that ensures a stable recovery of a sparse vector $\boldsymbol{s}$. A sufficient conditions for stable recovery is incoherence between the measurement matrix Φ and the matrix ψ. The stable recovery can be achieved by simply choosing a random measurement matrix [8, 9]. In particular, if the elements of Φ are chosen randomly as 1 or 0, then this is equivalent

to selecting a subset of antennas and frequencies to perform the measurements, which leads to a reduced set of measurements.

3.2 Multiple-View TWRI using CS

The previous subsection introduced CS for TWRI from a single vantage point. Multiple-view TWRI requires imaging to be performed from at least two different antenna arrays, which could simply amount to shifting the array to new locations or placing it along different walls. Several possible locations for the antenna setup for the multiple-view data acquisition are shown in Fig. 1.

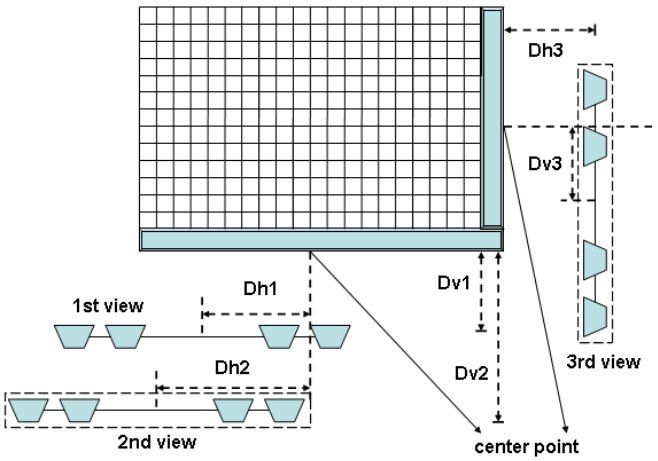

Figure 1 – Data acquisition from multiple-view TWRI.

When only one side of the enclosed structure is available, the multiple-view data can be acquired by synthesizing the same aperture according to different horizontal or vertical distances w.r.t the center point. For example, as seen in Fig .1, the first view is obtained by specifying the antenna array in the (Dh1, Dv1) position, where Dh1 and Dv1 denote the horizontal and vertical distances from the array to the center point and the edge of the wall, respectively. While shifting the same array to (Dh2, Dv2) position, the second view is available. Moreover, with access to other sides of the scene, the array can be deployed against different walls. The third view, for instance, is obtained from the 90 degree aspect angle.

One advantage of using multiple-view imaging is to overcome the lay-over or shadow effects when only a single view is available. This is due to the weak reflection of some targets compared to their surroundings. In some cases, targets of interest may be shadowed by other targets resulting in low radar signal returns. If the position of the antennas happen to be placed facing strong reflective obstacles, with the weak targets behind, it may result in some lay-over effects, rendering detection of the weak target difficult or impossible if only a single view is available. By contrast, information gathered from different views provides different perspectives, hence merging of multiple views can be very useful. However, according to the traditional image fusion, the obtained images from each single view require their own image registration before the final fusion operation. Accordingly, if data from a single view is incomplete or blurred, the performance of the fusion process will be compromised. Furthermore, since we need to image from each single view, system complexity and data processing time may become an impeding factor.

In this paper, we present a novel approach for the image fusion from multiple view data. This algorithm starts from building the relationship among different views of the same scene. Without loss of generality, we consider two views from the 0 and 90 degree aspect angles, respectively. Let $\boldsymbol{y}_1$ and $\boldsymbol{y}_2$ be the reduced measurement vectors obtained using CS, see Eq. (5), from $0°$ and $90°$ views, respectively:

$$\boldsymbol{y}_1 = \Phi_1 \psi_1 \boldsymbol{s}_1 = A_1 \boldsymbol{s}_1 \text{ and } \boldsymbol{y}_2 = \Phi_2 \psi_2 \boldsymbol{s}_2 = A_2 \boldsymbol{s}_2$$

Note that the measurement vector $\boldsymbol{s}_1$ is obtained by scanning the pixels from top to bottom, and left to right, as shown in Fig 2(a).

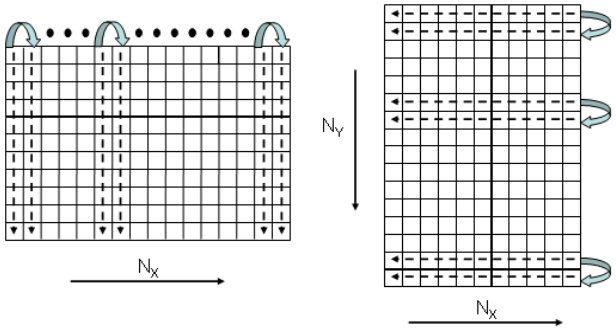

(a) (b)

Figure 2 – Pixel scanning: (a) $0°$ view and (b) $90°$ view.

When the second view is considered, the first pixel (first row and first column) in $\boldsymbol{s}_2$ corresponds to the pixel from $\boldsymbol{s}_1$ in the last row and first column. Similarly, the last pixel in $\boldsymbol{s}_2$ corresponds to the pixel in the first row and last column from $\boldsymbol{s}_1$. Naturally, we try to rearrange $\boldsymbol{s}_2$ and generate a new vector $\boldsymbol{s}_2^*$ subject to the pixels from $\boldsymbol{s}_2^*$ sharing the same sequence as $\boldsymbol{s}_1$. Fig.2 (b) demonstrates a simple rearrangement method to construct $\boldsymbol{s}_2^*$, where the pixels are extracted from right to left, and top to bottom. A pixels in $\boldsymbol{s}_1$ appears in the same location as in $\boldsymbol{s}_2^*$. Similarly, we construct the matrix ψ_2^* according to the same strategy. Therefore, we obtain

$$\boldsymbol{y}_2 = \Phi_2 \psi_2 \boldsymbol{s}_2 = \Phi_2 \psi_2^* \boldsymbol{s}_2^*$$

Consequently, we can employ the CS image formation algorithm to calculate a combined sparse representation for $\boldsymbol{s}_1$ and $\boldsymbol{s}_2^*$:

$$\boldsymbol{s} = \boldsymbol{s}_1 = \boldsymbol{s}_2^* .$$

Define a new measurement vector $\tilde{y}$ and matrices $\tilde{\Phi}$ and $\tilde{\psi}$ as follows:

$$\tilde{y} = \begin{bmatrix} y_1 \\ y_2 \end{bmatrix}, \quad \tilde{\Phi} = \begin{bmatrix} \Phi_1 & \mathbf{0} \\ \mathbf{0} & \Phi_2 \end{bmatrix}, \quad \tilde{\psi} = \begin{bmatrix} \psi_1 \\ \psi_2^* \end{bmatrix}$$

The composite measurement vector $\tilde{y}$ can be written as

$$\tilde{y} = \tilde{\Phi}\tilde{\psi}\,\boldsymbol{s}$$

A sparse solution for $\boldsymbol{s}$ can be obtained by solving the CS problem in (6), where hopefully the target locations can be revealed and false targets removed.

One of the advantages of this intelligent combination is to maintain all the collected data without losing potential information from a single view. Also, incorporating the available data from different views reduces the blurring effects in the case of two targets being close to each other, and hence providing more accurate evidence for target detections.

4. SIMULATION RESULTS AND DISCUSSION

The proposed algorithm is tested on synthesized through-the-wall radar data using different views. In this experiment we consider only point targets.

4.1 Experimental Setup

Since the multi-view TWRI requires placing the antennas in different locations, without loss of generality, we consider two different aspect angles: the $0°$ view (facing the front of the enclosed structure) and $90°$ view (rotating the array anti-clockwise by $90°$). We assume that the wall thickness and the dielectric constant of the wall material are known, and reflections from the front wall are eliminated. For the simulations we used a wall thickness 0.3m and a dielectric constant $\varepsilon = 6$. Furthermore, the array consists of 51 antennas spaced at 0.04 m intervals. The transmitted narrowband signals have frequencies ranging from 1 to 3 GHz, with 40-MHz frequency step: there are 51 frequencies in total. In each single view, we suppose that the middle of the wall (centre point) is the origin of coordinates. Consider the first view (from $0°$ aspect angle), the coverage of the down-range and cross-range is [-4.0545 m, 4.0545 m] and [0 m, 3.825 m], respectively. Three point targets are considered which are located at (-1.749 m, 0.525 m), (-0.477 m, 0.525 m), and (-0.477 m, 2.025 m), respectively. The three targets have the same reflection coefficients. Moreover, the size of the image pixel is set to (0.159 m ×0.075 m). Similarly, the corresponding parameter can be obtained for the second view (from the $90°$ angle) by simply exchanging the coordinates *x* and *y*. In both cases the centre of the array is 1.05 m away from the centre point of the wall.

4.2 Comparison and Analysis

To measure the error between the original scene and the reconstructed image, we use the Peak Signal-to-Noise Ratio (PSNR):

$$\mathrm{PSNR} = 20\log_{10}(255/\mathrm{RMSE})$$

where *RMSE* denotes the root-mean-square error. Figure 3(a) shows the original scene, which consists of three targets. From the $0°$ view and $90°$ view, only two targets are visible, the third target is obscured. However, the obscured target changes depending on the image view. As a consequence, the simple image fusion will not reveal the overlapped target. In fact if pixel-wise multiplication is employed, then the two obscured targets disappear in the fused image (Fig. 3(d)). Obviously, the pixel multiplication-based method only emphasizes the strong targets that appear in all views. The PSNR obtained by this multiplication-based method is only 64.12db.

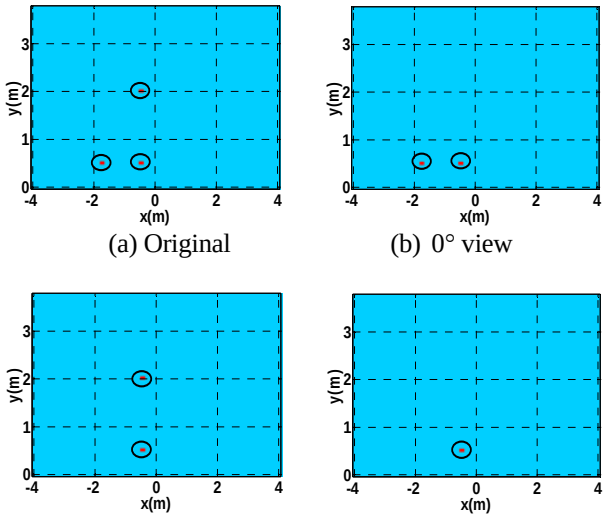

(a) Original (b) $0°$ view

(c) $90°$ view (d) Fused view

Figure 3 – TWRI from single views.

Figure 4 demonstrates the effectiveness of the proposed approach. Here, only 30 measurements are obtained from each view. CS is then applied to the composite measurement vector $\tilde{y}$. The simulation was run 10 times. A typical result is displayed in the top-left corner of Fig. 4. The other three images are obtained by applying different thresholds to the top-left image: the thresholds are set, respectively, at 10%, 15%, and 25% of the maximum magnitude. It's clear that the three targets are visible even before thresholding. The PSNR for the four images (Fig. 4(a), (b), (c) and (d)) is 72.69db, 73.10db, 73.15db and 73.21db, respectively. Compared to the traditional multiplication-based method, the proposed algorithm improves significantly the fusion performance. Again, we should note that the full data vector consists of $51 \times 51 = 2{,}601$ measurements.

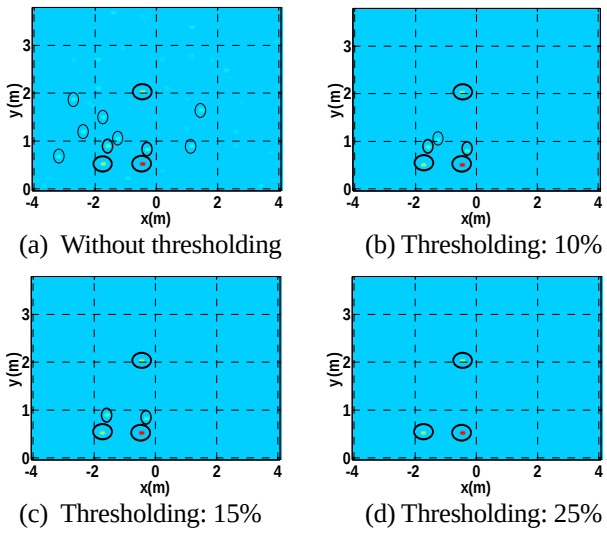

(a) Without thresholding (b) Thresholding: 10%

(c) Thresholding: 15% (d) Thresholding: 25%

Figure 4 – Target Detection using multi-view CS.

From the above results, the following observations are in order:

(1) Prior to applying the proposed multi-view CS algorithm, a new measurement vector $\tilde{y}$ and dictionary $\tilde{\Phi}\tilde{\psi}$ need to be constructed as described in Section 3.2. The proposed algorithm only requires solving the CS problem once, instead of calculating each single view separately. By doing so, significant computational savings can be achieved.

(2) Some false targets may appear initially as shown in the first image in Fig. 4. However, we can notice that the difference in intensity between the false targets and the actual targets is obvious; the false targets are much weaker and can be removed with simple thresholding.

5. CONCLUSION

A new approach for the multi-view through-the-wall radar imaging using compressed sensing was presented in this paper. A novel image fusion strategy was developed, which combines the measurement data from different views into a composite measurement vector, and then applies CS to solve the image formation problem. Finally, simulation results were provided which clearly demonstrate the effectiveness of the proposed method; it achieves much higher reconstruction accuracy compared to the alternative approach of image formation followed by fusion.

ACKNOWLEDGMENTS

This work is supported in part by the Australian Research Council.

REFERENCES

[1] Special issue of *IEEE Transactions on Geosciences and Remote Sensing*, M. Amin and K. Sarrabandi, guest editors, Vol. 47, no. 5, May 2009.

[2] Special issue of *Journal of the Franklin Institute*, M. Amin, guest editor, Volume 345, no. 6, Sep. 2008.

[3] F. Ahmad and M. G. Amin, "Wideband synthetic aperture imaging for urban sensing applications," *Journal of the Franklin Institute*, vol. 345, no. 6, pp. 618–639, Sep. 2008.

[4] D. Donoho, "Compressed sensing," *IEEE Trans. Information Theory*, vol. 52, pp. 1289-1306, 2006.

[5] E. J. Candes, J. Romberg and T. Tao, "Robust uncertainty principles: exact signal reconstruction from highly incomplete frequency information," *IEEE Trans. Informatin Theory*, vol. 52, pp. 489-509, 2006.

[6] H. Rauhut, K. Schnass and P. Vandergheynst, "Compressed Sensing and Redundant Dictionaries," *IEEE Trans. Inform. Theory*, vol. 54, pp. 2210-2219, May 2008.

[7] Y.-S. Yoon and M. Amin, "Compressed sensing technique for high-resolution radar imaging," in *Proc. of SPIE Signal Processing, Sensor Fusion, and Target Recognition* XVII, Vol. 6958, Orlando, FL, Mar. 2008.

[8] Y.-S. Yoon and M. G. Amin, "Through-the-wall radar imaging using compressive sensing along temporal frequency domain," in *Proc. IEEE Int. Conf. Acoustics, Speech and Signal Processing* (ICASSP 2010), Dallas, TX, USA, March 14–19, 2010.

[9] Q. Huang, L. Qu, B. Wu and G. Fang, "UWB through-wall imaging based on compressive sensing," *IEEE Trans. Geoscience and Remote Sensing*, Vol. 48, no.3, pp. 1408–1415, Mar. 2010.

[10] A. C. Gurbuz, J. H. McClellan and W. R. Scott, "A compressive sensing data acquisition and imaging method for stepped frequency GPRs," *IEEE Trans. Signal Processing*, Vol. 57, no. 7, pp. 2640–2650, July 2009.

[11] C. Debes, M. G. Amin, and A. M. Zoubir, "Target detection in single- and multiple-view through-the-wall radar imaging," IEEE *Trans. Geoscience and Remote Sensing*, vol. 47 (5), pp. 1349–1361, 2009.

[12] F. Ahmad, M. G. Amin, and S. A. Kassam, "A beamforming approach to stepped-frequency synthetic aperture through-the-wall radar imaging," in *Proc. IEEE Inter. Workshop on Computational Advances in Multi-Sensor Adaptive Processing*, pp. 24 - 27, 2005.